Lipid-Free Structure and Stability of Apolipoprotein A-I: Probing the Central Region by Mutation†

Irina N. Gorshkova,*,‡,§ Tong Liu,§ Vassilis I. Zannis,§ and David Atkinson‡

Department of Physiology and Biophysics and Section of Molecular Genetics, Whitaker Cardiovascular Institute, Departments of Medicine and Biochemistry, Boston University School of Medicine, 715 Albany Street, Boston, Massachusetts 02118

Received March 13, 2002; Revised Manuscript Received June 7, 2002

ABSTRACT: To probe the structure and stability of the central region of lipid-free apolipoprotein (apo) A-I (residues 123−165), we studied the effects of four mutations made in this region on the conformation, stability, dimyristoylphosphatidylcholine (DMPC) binding kinetics, and size of discoidal reconstituted high-density lipoprotein (rHDL) particles. The apoA-I deletion Δ(144−165) leads to a red shift in the wavelength of maximum fluorescence and a reduction in the α-helical content, the stability, the initial rate of association with DMPC liposomes, and the size of the discoidal particles. The data are consistent with the helical structure of residues 144−165, and the deletion appears to perturb the tertiary organization of the N-terminal half of apoA-I. In contrast, the deletion of the adjacent region, Δ(136−143), leads to stabilization without altering the number of residues in the helical conformation or the initial rate of association with DMPC liposomes. The quadruple substitution E125K/E128K/K133E/E139K leads to ∼17 additional residues in the helical conformation and an increase in the stability, the initial rate of association with DMPC liposomes, and the size of the rHDL particles. The findings are consistent with the disordered structure of the segment of residues 123−142, which becomes helical as a result of the quadruple mutation or upon lipid binding. The naturally occurring mutation L141R (also associated with coronary heart disease) that is located in this segment does not change the protein conformation but leads to a reduced stability and a decreased rate of association with DMPC liposomes that may relate to the observed altered functions of this mutant.

Human apolipoprotein (apo)[1] A-I is the major protein constituent of high-density lipoprotein (HDL) that determines the structure and function of the HDL particles (*1*). Lipid-bound apoA-I and lipid-free apoA-I participate in reverse cholesterol transport via their interactions with scavenger receptor class B type 1 (SR-B1) and ATP-binding cassette transporter 1 (ABCA1) (*2*, *3*), respectively. Up to 13−15% of apoA-I is present in plasma in a lipid-free or lipid-poor state and is the most effective acceptor of cell cholesterol and phospholipids (*4*). The correct conformation of apoA-I has been shown to be crucial for the efficient functioning of the protein (*2*, *3*, *5*−*9*). While intensive studies of reconstituted HDL (rHDL) provided valuable information about conformation, stability, and the structure−function relationships of apoA-I in the lipid-bound state (*5*, *6*, *8*, *10*−*12*), the conformation and stability of lipid-free apoA-I have not been fully understood.

The 243-amino acid polypeptide chain of apoA-I is organized into repeated homolologous 11- and 22-residue putative amphipathic helices punctuated by prolines. So far, no X-ray crystal structure of full-length apoA-I is available, and the majority of information, which leads to a detailed understanding of the conformation and structure−function relationships of apoA-I, comes from studies of bioengineered mutant apoA-I forms (reviewed in refs *2*, *3*, and *13*). Mutation of the N-terminus of apoA-I has shown that the 43 N-terminal residues are critical for the solution structure and stability of the protein, and that deletion of residues 88−98 affects dramatically both the solution and the lipid-bound conformation of apoA-I (*14*). Our recent studies probing the conformation and stability of apoA-I by mutation of the C-terminus suggested the presence of stable helical structure in the region of residues 165−243 of lipid-free apoA-I (*15*), in agreement with the secondary structural prediction based on the apoA-I sequence (*16*) and the secondary structure determined from the crystal structure of the truncated (44−243) apoA-I (*17*).

In the current study, we have probed the conformation and stability of the middle region of lipid-free apoA-I, the segment of residues 123−165. This segment has been shown to be of great importance for the function of apoA-I. Various deletion and substitution mutations of this segment reduce

† This work was supported by PO1HL 26335 and Grant HL 48739 from the National Institutes of Health.

* To whom correspondence should be addressed: Department of Physiology and Biophysics, Boston University School of Medicine, 715 Albany St., W-322, Boston, MA 02118. Fax: (617) 638-4041. Phone: (617) 638-4207. E-mail: igorshko@bu.edu.

‡ Department of Physiology and Biophysics, Boston University School of Medicine.

§ Departments of Medicine and Biochemistry, Boston University School of Medicine.

[1] Abbreviations: apo, apolipoprotein; CD, circular dichroism; DMPC, dimyristoylphosphatidylcholine; GdnHCl, guanidine hydrochloride; HDL, high-density lipoprotein(s); LCAT, lecithin:cholesterol acyltransferase; POPC, palmitoyloleoylphosphatidylcholine; rHDL, reconstituted high-density lipoprotein(s); rTEV protease, recombinant tobacco-etched viral protease; WMF, wavelength of maximum fluorescence; WT, recombinant human wild-type apoA-I.

10.1021/bi025807d CCC: $22.00
Published on Web 07/26/2002

dramatically the lecithin:cholesterol acyltransferase (LCAT) activating ability of apoA-I (*6*−*8*, *18*−*21*). The region of residues 122−186 has been shown to be important for interaction of apoA-I with phospholipids in vitro (*22*), and residues 100−143 are necessary for efficient binding of apoA-I to lipids and for stabilization of lipoprotein particles in vivo (*23*). A full understanding of the relationship between structural changes in the central part of apoA-I and the functions of the protein requires a detailed understanding of the conformation of this region of apoA-I.

The model for lipid-free apoA-I proposed by Roberts et al. (*24*) based on limited proteolysis data suggests that residues 126−135 and 144−189 form two helices, correspondingly, which are connected by a loop formed by residues 136−143. The secondary structure model of apoA-I proposed by Nolte and Atkinson (*16*), based on the apoA-I sequence and CD data for apoA-I−dimyristoylphosphatidylcholine (DMPC) complexes, predicts that residues 123−164 form two helices, helix 5 (residues 123−142) and helix 6 (residues 145−164), punctuated by a loop region consisting of Pro143 and Leu144. Our previous studies (*15*) suggest that the secondary structure of lipid-free apoA-I may differ from this predicted conformation of lipid-bound apoA-I by unfolding of one central helix, which may be helix 5 or 6.

To probe the secondary structure of residues 123−165, we made two deletion and two amino acid substitution mutations in this region. In a Δ(144−165) apoA-I mutant, we deleted putative helix 6 with the adjacent Leu144 and Pro165, and in a Δ(136−143) mutant, we deleted the C-terminal part of the putative helix 5 with the adjacent Pro143. In an amino acid E125K/E128K/K133E/E139K substitution mutant, we reversed the electrostatic charge of four residues of the putative helix 5. This mutant was designed to make the charge distribution of repeat 121−142 (putative helix 5) similar to that of repeat 139−160 of the apoE3 22 kDa fragment. A single-amino acid substitution L141R generated a naturally occurring apoA-I mutant, which is associated with coronary heart disease and has been shown to reduce the ability of apoA-I to promote cholesterol efflux and to activate LCAT (*2*). We studied the effects of the mutations on the conformation and stability of lipid-free apoA-I, as well as on the initial rate of association of the protein with DMPC liposomes and the size of discoidal palmitoyloleoylphosphatidylcholine (POPC)−cholesterol−apoA-I particles. Our observations are consistent with the helical structure of residues 145−164 and the disordered structure of residues 123−142 in lipid-free apoA-I.

MATERIALS AND METHODS

Cell culture reagents, oligonucleotides for polymerase chain reaction, DH10Bac *Escherichia coli* competent cells, and rTEV protease were purchased from GIBCO BRL Life Technologies, Inc. (Grand Island, NY). Vent polymerase, T4 ligase, and restriction enzymes were purchased from New England Biolabs (Beverly, MA). Other materials for the polymerase chain reaction were obtained from Perkin-Elmer (Boston, MA). Monoclonal anti-human apoA-I antibodies were purchased from Ottawa Heart Institute (Ottawa, ON). Bactotryptone and bacto-yeast extract were obtained from VWR (Pittsburgh, PA). Ni−NTA resin was purchased from Qiagen Inc. (Hilden, Germany). High-molecular mass calibration proteins for gradient gel electrophoresis were purchased from Pharmacia Biotech (Piscataway, NJ). All other reagents were of the highest available quality.

Generation of Expression Plasmids, Expression of Recombinant ApoA-I in the Baculovirus System, and Protein Purification. Generation of baculovirus-expressing wild-type apoA-I (WT) was performed as reported previously (*25*). Mutant forms of apoA-I were produced in a similar manner. Briefly, the human apoA-I cDNA was mutagenized by polymerase chain reaction, using a set of specific mutagenesis primers, containing the mutation of interest, and a set of flanking universal primers containing the restriction sites *Bam*HI and *Sal*I, using the pBluescript-AI cDNA plasmid as a template. The set of universal primers included 5′-ACT CAA GGA TCC GAT GAA CCC CCC CAG AGC CCC TGG GAT-3′ (sense) and 5′-ACT CAA GTC GAC TTT TTC CCA CTT TGG AAA CGT TTA TTC TGA GCA-3′ (antisense). Specifically, we used 5′-GAG AAG CTG AGC CCA TAC AGC GAC GAG CT-3′ (sense) and 5′-AG CTC GTC GCT GTA TGG GCT CAG CTT CTC-3′ (antisense) primers for the mutagenesis of Δ(144−165) apoA-I, 5′-GC CAG AAG CTG CAC CTG GGC GAG GAG AT-3′ (sense) and 5′-AT CTC CTC GCC CAG GTG CAG CTT CTG GC-3′ (antisense) primers for the mutagenesis of Δ(136−143) apoA-I, and 5′-CTG CAA GAG AAG CGG AGC CCA CTG GGC-3′ (sense) and 5′-GCC CAG TGG GCT CCG CTT CTC TTG CAG-3′ (antisense) primers for the mutagenesis of L141R apoA-I. For the mutagenesis of E125K/E128K/K133E/E139K apoA-I, 5′-CTG CGC GCA AAG CTC CAA AAG GGC GC-3′ (sense) and 5′-GC GCC CTT TTG GAG CTT TGC GCG CAG-3′ (antisense) primers were used initially to generate the plasmid pFAST-AI that carried the E125K and E128K mutations. Then 5′-CAG GAG CTG CAC GAG CTG CAA AAG AAG-3′ (sense) and 5′-CTT CTT TTG CAG CTC GTG CAG CTC CTG-3′ (antisense) primers were used to further mutagenize apoA-I cDNA (K133E/E139K) using the plasmid pFAST-AI(E125K/E128K) as a template. The DNA fragment containing the mutation of interest was digested with *Bam*HI and *Sal*I, and cloned into the corresponding sites of the pFASTBAC donor plasmid. The DNA of each mutant in the resulting pFASTBAC−apoA-I constructs was completely sequenced using the Core for DNA Sequencing, Department of Biochemistry, Boston University School of Medicine. Cells containing recombinant bacmids were selected by kanamycin, tetracycline, and gentamycin resistance as white colonies due to the disruption of the *LacZ* sequence in the recombinant bacmid. Recombinant bacmid DNA was isolated by minipreps and used to transfect a monolayer of Sf-9 insect cells (*26*). Recombinant viruses were isolated, amplified, titrated, and used to infect larger amounts of Sf-9 cells grown in suspension in Sf-900 II serum-free medium at 27 °C. Infected Sf-9 cells were pelleted and resuspended in a lysis buffer. The supernatant obtained after sonication followed by centrifugation of the cell pellet was used for the purification of apoA-I fusion proteins using a Ni^{2+}−nitrilotriacetic acid resin affinity column (*27*). At this stage, the purified protein could be lyophilized and stored at −80 °C. For use in the experiments, the lyophilized protein was solubilized and the His tag was cleaved using recombinant tobacco-etched viral (rTEV) protease. Since rTEV protease is a highly site specific protease (*28*, *29*), and there is no recognition site for rTEV in the

apoA-I sequence, the cleavage does not result in any degradation of apoA-I. The His tag-free protein was purified using a second Ni^{2+}−nitrilotriacetic acid resin affinity column. The cleaved His tag fragments, undigested apoA-I fusion proteins, and rTEV protease, which itself contains the His tag, remained bound to the Ni^{2+}−nitrilotriacetic acid column, while pure His tag-free apoA-I was eluted from the column. The purified apoA-I was analyzed by 12% SDS−PAGE followed by staining with Coomassie Brilliant Blue R-250 and by Western blotting using monoclonal antibodies against human apoA-I. The protein concentration after the purification was 0.3−0.5 mg/mL. The purified protein was refolded at a concentration of ∼0.1 mg/mL by subsequent dialysis against 4, 2.5, and 1.25 M GdnHCl solutions in PBS [0.15 M NaCl, 10 mM sodium phosphate, 0.01% EDTA, and 0.02% NaN_3 (pH 7.4)], followed by extensive dialysis against the appropriate buffer [10 mM sodium phosphate and 0.02% NaN_3 (pH 7.4) for CD experiments or PBS for fluorescence and DMPC binding measurements]. The concentration of the refolded protein (∼0.1 mg/mL) was lower than the critical concentration of plasma apoA-I self-association (∼0.3 mg/mL) under the ionic strength and pH conditions used in our experiments (*30*). Our far-UV CD analysis of the proteins performed at several protein concentrations, including 0.1 mg/mL (given below), is consistent with the absence of protein self-association at the concentration used for protein refolding. Protein concentrations were determined by modified Lowry and BCA protein assays (Pierce, Rockford, IL).

Circular Dichroism Spectroscopy. CD measurements were performed on an AVIV 62DS spectropolarimeter (AVIV Associates, Inc.) equipped with a thermoelectric temperature control and calibrated with *d*-10-camforsulfonic acid, in 5, 2, or 1 mm path length quartz cuvettes, at a protein concentration of 25−100 μg/mL. Far-UV CD spectra were recorded as described previously (*15*). For each protein, spectra were recorded at several protein concentrations within the indicated range and then normalized to molar residue ellipticity, using a mean residue weight of 115.0 for the wild type, 113.0 for Δ(144−165), 114.4 for Δ(136−143), 115.0 for E125K/E128K/K133E/E139K, and 115.1 for L141R. The complete superposition of the normalized spectra obtained at various protein concentrations for each recombinant apoA-I is consistent with the absence of protein self-association within the range of protein concentrations used in our experiments. The α-helix content was estimated from the molar residue ellipticity at 222 nm, [Θ_{222}] (*31*). Protein concentrations in samples were determined before and after CD experiments, and the values agreed within 5%.

Thermal and Chemical Unfolding Monitored by CD. Monitoring of thermal and chemical unfolding of apoA-I by ellipticity at 222 nm was performed as described previously (*15*), at protein concentrations of 25−80 μg/mL. The complete superimposition of the thermal and chemical denaturation curves obtained at several protein concentrations for each recombinant protein is, again, consistent with the absence of protein self-association. The midpoint (melting temperature), T_m, and van't Hoff enthalpy, ΔH_v, of the temperature-induced transitions were determined from van't Hoff plots (*32*) of ln K_{eq} versus $1/T$, where K_{eq} is the apparent equilibrium constant and T is the temperature in kelvin. The equilibrium constant was calculated as $K_{eq}(T) = (\Theta_F - \Theta_{obs})/(\Theta_{obs} - \Theta_U)$, where Θ_{obs} is the observed ellipticity and Θ_F and Θ_U are baselines for the protein folding and unfolding states determined by linear extrapolations of the pre- and post-transitional regions, respectively. In the transition region, the plots were fitted by the linear function $\ln K_{eq} = \Delta S/R - (\Delta H_v/R) \times 1/T$, where R (1.98 cal mol^{-1} K^{-1}) is the universal gas constant and ΔS is the transition entropy.

For chemical unfolding, the free energy of denaturation (conformational stability), $\Delta G_D°$, the midpoint of denaturation, $D_{1/2}$, and m, which reflects the steepness of the denaturation curve in the transition region, were determined using a linear extrapolation method (*33*). A plot of Gibbs free energy ΔG_D ($= -RT \ln K_{eq}$, where $T = 25$ °C $= 298.15$ K) versus denaturant concentration, [D], was fitted by the linear function $\Delta G_D = \Delta G_D° - m[D]$. The apparent equilibrium constant, K_{eq}, was calculated as shown above, except $\Theta_{obs}([D])$ is the observed ellipticity at a given concentration of GdnHCl, [D], and Θ_F and Θ_U are the ellipticities in the folded and unfolded states, respectively. Θ_F and Θ_U were taken to be constants, since linear extrapolation of the pre- and post-transitional regions of the denaturant unfolding curves leads to poorer accuracy of the estimations due to a small number of points in these regions (that is not the case for the thermal unfolding curves).

Fluorescence Spectroscopy. All fluorescence experiments were carried out at 25 °C and at a protein concentration of 0.06 mg/mL. On the basis of our CD analysis, the proteins are monomeric at this concentration. Intrinsic Trp fluorescence spectra were measured with a FluoroMax-2 fluorescence spectrophotometer (Instruments S.A., Inc., Jobin Yvon/Spex Division) using 5 nm excitation and 2.5 nm emission slit widths, and a 295 nm excitation wavelength to avoid Tyr fluorescence. The emission was scanned from 300 to 380 nm. The wavelength of maximum fluorescence (WMF) of the Trp residues was determined from uncorrected spectra after subtraction of the buffer baseline. For monitoring chemical unfolding by WMF, proteins were incubated with GdnHCl as for CD-monitored unfolding. $\Delta G_D°$, $D_{1/2}$, and m were determined as described above for CD-monitored unfolding, with WMF being used instead of ellipticity in the equation for K_{eq}.

DMPC Clearance Kinetic Analysis. The initial rate of binding of WT and mutant proteins to DMPC multilamellar liposomes was studied using a kinetic−turbidimetric method (*34*). Briefly, 250 μg of DMPC in a chloroform/methanol (2:1) solution was dried under nitrogen and resuspended in 900 μL of PBS by vortexing to form liposomes. Then, 100 μg of apoA-I in PBS was added to the lipid emulsion to give a DMPC:apoA-I ratio of 2.5:1 (w/w) and an apoA-I concentration of 0.1 mg/mL. The DMPC clearance was followed by monitoring the decrease in absorbance at 325 nm at 2 min intervals at 24 °C. A plot of absorbance at 325 nm versus time in minutes, $A(t)$, was fitted by the exponential decay function $A(t) = A_\infty + ae^{-t/k}$, where A_∞, a, and k are fitting parameters. Half-times ($t_{1/2}$), corresponding to a 50% decrease in absorbance, were determined for each protein.

Preparation and Gradient Gel and Electron Microscopy Analysis of rHDL Containing POPC, Cholesterol, and ApoA-I. rHDL particles were prepared by the sodium cholate dialysis method (*35*), using the POPC/cholesterol/apoA-I/sodium cholate molar ratio of 100:10:1:100, as previously described (*36*). The lipid-free apoA-I that was not incorporated in the lipid−protein complexes was removed by dialysis

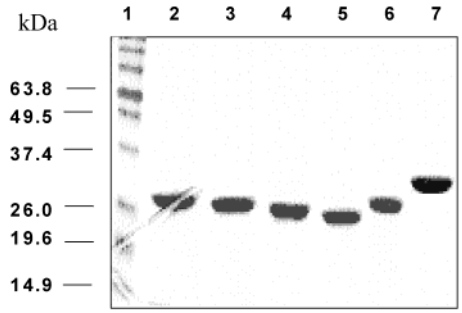

FIGURE 1: SDS−PAGE (12%) analysis of purified recombinant apoA-I. In lane 1 are molecular mass markers (masses in kilodaltons). Proteins in lanes 2−6 are apoA-I purified after cleavage of the His tag: lane 2, E125K/E128K/K133E/E139K; lane 3, L141R; lane 4, Δ(136−143); lane 5, Δ(144−164); and lane 6, WT apoA-I. Lane 7 contains WT apoA-I purified before cleavage of the His tag.

overnight against PBS buffer at 4 °C with at least three changes of 4 L each, using dialysis tubing with a 50 000 Da molecular mass cutoff. Gel filtration of the complexes isolated from this preparation on an Amersham Pharmacia Biotech Superose 6HR column, 10/30, driven by a Pharmacia FPLC system, showed that all unbound proteins were removed during the dialysis, and the complexes were not contaminated with lipid-free apoA-I. Apolipoprotein−lipid complex formation was verified by analysis with nondenaturing polyacrylamide gradient (8 to 25%) gel electrophoresis using small-format gels immobilized to plastic backing (Pharmacia Phast gel system, Pharmacia Biotech). A range of the hydrodynamic diameter of the complexes was estimated from the gels using high-molecular mass calibration proteins. rHDL were observed under the electron microscope to analyze the morphology of the complexes and estimate their average diameter. Each rHDL sample was either processed without dilution or diluted with deionized water to a final protein concentration of approximately 0.5 mg/mL. A 5 μL aliquot of each vesicle suspension was applied for 10 s to a Formvar carbon-coated 300 mesh copper grid. The carbon film surface was previously made hydrophilic by glow discharging in a Balzers Union CTA 010 Glow Discharge apparatus (Bal-Tec Products, Middlebury, CT) and used immediately. Excess rHDL suspension was blotted with filter paper and immediately replaced with a 5 μL droplet of 1% sodium phosphotungstate (pH 7.4). After a few seconds, excess stain was blotted and the grid was air-dried. Images of random fields of particles were recorded on S0163 film (Eastman Kodak, Rochester, NY) in a Philips CM12 electron microscope (Philips Electron Optics, Eindhoven, The Netherlands), developed in D19 developer, and scanned on an Eversmart Supreme Scanner (CreoScitex Corp. Ltd., Vancouver, BC). The major diameter of rHDL particles was determined from negative staining microscopy as an average diameter of 100 particles.

RESULTS

Expression and Purification of Recombinant ApoA-I. Up to 20 mg of pure recombinant protein was obtained from the cell lysate of 1 L of culture medium after cleavage of the His tag. The purity and identity of each recombinant protein after cleavage of the His tag were assessed by SDS−PAGE and Western blotting. Figure 1 shows 12% SDS−PAGE analysis of the proteins purified after the cleavage of the His tag (lanes 2−6). The molecular masses of the mutant proteins estimated from the gels are consistent with those predicted from the nature of the mutations. For comparison, lane 7 of the gel was loaded with WT apoA-I before the cleavage of the His tag. The molecular masses of undigested fusion apoA-I estimated from gels are higher than those of the corresponding His tag-free proteins, in accordance with the molecular mass of the His tag. The analysis of the purified proteins after the cleavage of the His tag does not show the presence of the corresponding undigested fusion proteins. Western blot analysis showed that all the purified proteins were immunologically identical to apoA-I. The purity of the recombinant apoA-I used in our studies was 95−97%.

α-*Helical Content.* The normalized far-UV CD spectra of WT and variant forms of apoA-I (not shown) were used to estimate the α-helical content in the secondary structure of the proteins, from which an estimate of the number of helical residues was derived (Table 1). The deletion Δ(144−165) leads to a small (∼4%) but statistically significant reduction in the α-helical content that corresponds to the loss of ∼22 residues in the helical conformation. In contrast, the deletion of the adjacent segment Δ(136−143) leads to a small (∼3%) but statistically significant increase in the α-helical content that corresponds to an unaltered number of residues in the helical structure of the protein. The quadruple point mutation E125K/E128K/K133E/E139K leads to an ∼7% increase in the α-helical content, which corresponds to a gain of ∼17 residues in the helical conformation. Point mutation L141R does not lead to statistically significant changes in α-helical content.

Thermal and Denaturant-Induced Unfolding Monitored by CD. The thermal unfolding curves monitored by ellipticity at 222 nm, $[\Theta_{222}](T)$, are shown in Figure 2; the corresponding van't Hoff plots, ln K_{eq} $(1/T)$, are shown in the inserts, and the values of the melting temperature, T_m, and the effective enthalpy, ΔH_v, determined by the van't Hoff analysis are given in Table 1. The equilibrium character and reversibility of thermal unfolding were confirmed as previously described (*15*). The deletion Δ(144−165) leads to an ∼5 °C decrease in T_m, an indication of the destabilizing effect of the mutation, and an ∼14 kcal/mol reduction in ΔH_v, suggesting a lower cooperativity of the thermal transition compared to that for WT. The shape of the melting curve for the deletion Δ(144−165) also suggests a significantly lower cooperativity of the thermal transition. In contrast, deletion of the adjacent segment, Δ(136−143), leads to an ∼3 °C increase in T_m, indicating a small but significant stabilizing effect of the mutation. The E125K/E128K/K133E/E139K mutation leads to a small (∼2 °C) but reproducible increase in T_m, indicating the small but significant stabilizing effect of these amino acid substitutions. van't Hoff analysis of the melting curves for the L141R substitution mutant does not show statistically significant alterations in T_m, but gives a reduced value for ΔH_v, suggesting a slightly lower cooperativity of the thermal transition for this mutant.

Chemical unfolding curves monitored by ellipticity at 222 nm are shown in Figure 3A, and the conformational stability, $\Delta G_D°$, the midpoint of chemical denaturation, $D_{1/2}$, and m values determined from the curves are listed in Table 1. The denaturation curve of the Δ(144−165) mutant is shifted

Table 1: α-Helical Content and Thermodynamic Parameters of WT and Variant ApoA-Is Determined by Far-UV CD[a]

protein	α-helix[b] (%)	no. of residues[c] in protein	no. of residues[c] in helix[d]	T_m[e] (°C)	ΔH_v[e] (kcal/mol)	$\Delta G_D°$[f] (kcal/mol)	m[f] [kcal (mol of apoA-I)$^{-1}$ (mol of GndHCl)$^{-1}$]	$D_{1/2}$[f] (M)
WT	58	248	∼144	59 ± 1	40 ± 1	2.5 ± 0.1	2.4 ± 0.1	1.0 ± 0.05
Δ(144−165)	54*	226 (−22)	∼122 (−22)	54 ± 2*	26 ± 1***	2.0 ± 0.2*	2.7 ± 0.2	0.7 ± 0.04**
Δ(136−143)	61*	240 (−8)	∼146 (∼0)	62 ± 1*	41 ± 3	3.2 ± 0.3*	2.8 ± 0.3	1.1 ± 0.03
E125K/E128K/K133E/E139K	65*	248 (0)	∼161 (17)	61 ± 0.0*	37 ± 1.6	3.1 ± 0.1*	2.8 ± 0.2	1.1 ± 0.07
L141R	56	248 (0)	∼139 (−5)	57 ± 1	37 ± 1*	2.2 ± 0.1*	2.3 ± 0.1	0.9 ± 0.03

[a] Values are averages ± the standard deviation from three to six experiments for two or three independent preparations of each protein. Significant differences from the value for WT: one asterisk, $p < 0.05$; three asterisks, $p < 0.005$. [b] Estimated from the $[\Theta_{222}]$ value at 25 °C according to ref *31*; the systematic error of the estimation is ±3%, and the statistical error is within ±1−3%. [c] Values in parentheses show changes in the number of residues as compared to that for WT. [d] Determined by multiplying the number of residues in the protein by its α-helical content. [e] The melting temperature T_m and effective enthalpy ΔH_v of thermal unfolding were determined from van't Hoff analysis of the melting curves monitored by ellipticity at 222 nm. [f] The conformational stability, $\Delta G_D°$, midpoint of chemical denaturation, $D_{1/2}$, and m values were determined by the linear extrapolation method from CD-monitored chemical unfolding curves.

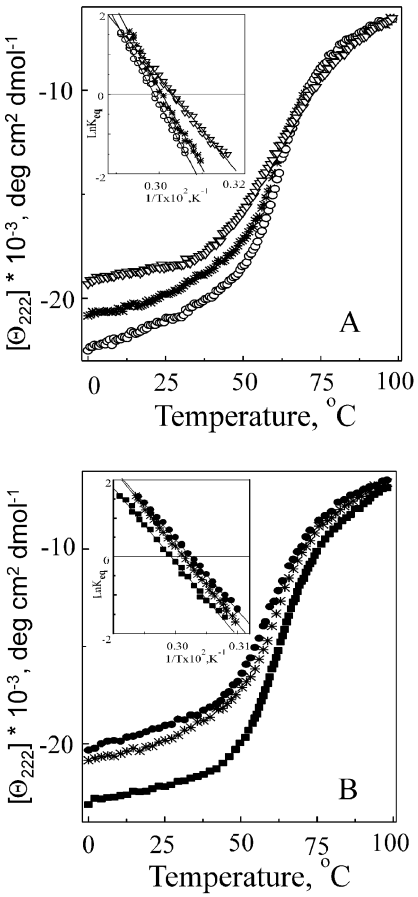

FIGURE 2: Thermal unfolding of recombinant apoA-I monitored by the ellipticity at 222 nm. (A) The deletion mutations Δ(144−164) (▽) and Δ(136−143) (○). (B) The amino acid substitution mutations E125K/E128K/K133E/E139K (■) and L141R (●). WT (∗) is shown for comparison in each panel. The insets show the corresponding van't Hoff plots (ln K_{eq} vs 1/T).

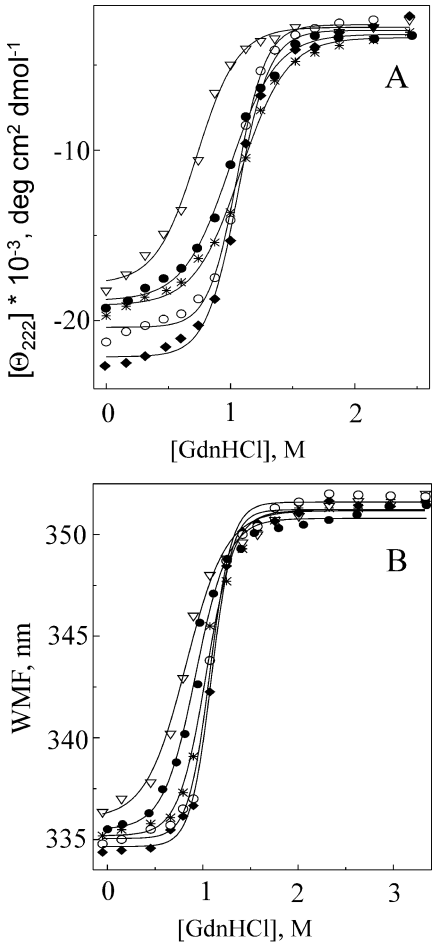

FIGURE 3: Denaturant-induced unfolding of recombinant forms of apoA-I monitored by the ellipticity at 222 nm (A) and by fluorescence emission (B): WT (∗), Δ(144−165) (▽), Δ(136−143) (○), E125K/E128K/K133E/E139K (◆), and L141R (●).

significantly to lower concentrations of denaturant compared to that of WT, in accordance with an ∼0.3 M reduction in $D_{1/2}$. This mutation leads also to an ∼0.5 kcal/mol reduction in $\Delta G_D°$, indicating a large destabilizing effect of the Δ(144−165) deletion. In contrast, deletion of the adjacent region in the Δ(136−143) mutant leads to protein stabilization, as indicated by an ∼0.7 kcal/mol increase in the conformational stability $\Delta G_D°$. Similarly, the two point substitution mutations have opposite effects on protein stability. The E125K/E128K/K133E/E139K mutation leads to an ∼0.6 kcal/mol increase in the conformational stability $\Delta G_D°$, suggesting a stabilizing effect of this quadruple amino acid substitution. The single-amino acid substitution L141R leads to destabilization of apoA-I, as indicated by an ∼0.3 kcal/mol reduction in $\Delta G_D°$.

Fluorescence Studies. Importantly, none of the mutations that were studied alters the total number of tryptophans located at positions 8, 50, 72, and 108. Values of WMF determined from fluorescence emission spectra of the proteins are shown in Table 2. WT, Δ(136−143), E125K/E128K/K133E/E139K, and L141R apoA-I exhibit similar values of WMF (335 nm), indicating relatively hydrophobic

Table 2: WMF and Thermodynamic Parameters of WT and Variant ApoA-Is Determined from Tryptophan Fluorescence[a]

protein	WMF[b] (nm)	$\Delta G_D°$ [c] (kcal/mol)	m [c] [kcal (mol of apoA-I)$^{-1}$ (mol of GndHCl)$^{-1}$]	$D_{1/2}$ [c] (M)
WT	335	4.0 ± 0.1	3.7 ± 0.2	1.1 ± 0.04
Δ(144−165)	336.5	2.2 ± 0.3***	2.6 ± 0.2**	0.8 ± 0.05**
Δ(136−143)	335	4.0 ± 0.3	3.6 ± 0.3	1.1 ± 0.06
E125K/E128K/K133E/E139K	335	4.3 ± 0.1*	4.0 ± 0.2	1.1 ± 0.05
L141R	335	3.0 ± 0.3*	3.2 ± 0.2*	0.9 ± 0.06*

[a] Values are averages ± the standard deviation from three to six experiments for two or three independent preparations of each protein. Significant differences from the value for WT: one asterisk, $p < 0.05$; three asterisks, $p < 0.005$. [b] The systematic and statistical error of measurements of WMF is ±0.5 nm. [c] The conformational stability, $\Delta G_D°$, midpoint of chemical denaturation, $D_{1/2}$, and m values were determined by the linear extrapolation method from fluorescence-monitored chemical unfolding curves.

environments of Trp residues that are likely maintained by intraprotein contacts. In contrast, the Δ(144−165) mutant exhibits a red shift in WMF, suggesting slightly more polar environment of Trp residues in this deletion mutant.

Chemical unfolding curves monitored by WMF are presented in Figure 3B, and the thermodynamic parameters derived from these data are shown in Table 2. The Δ(144−165) mutation leads to a large reduction in the conformational stability $\Delta G_D°$ (∼1.8 kcal/mol), midpoint of denaturation $D_{1/2}$ (∼0.3 M), and m value [∼1.1 kcal (mol of apoA-I)$^{-1}$ (mol of GdnHCl)$^{-1}$], indicating a significant destabilizing effect of the Δ(144−165) deletion. Deletion of the adjacent segment in the Δ(136−143) mutant does not alter the protein stability monitored by WMF. The E125K/E128K/K133E/E139K mutant shows an ∼0.3 kcal/mol increase in $\Delta G_D°$, indicating a small stabilizing effect of the quadruple-point substitution. In contrast, the L141R mutant shows an ∼1.0 kcal/mol reduction in $\Delta G_D°$ and an ∼0.2 M reduction in $D_{1/2}$, indicating a destabilizing effect of the single-point substitution.

Kinetics of Binding of ApoA-I to DMPC Liposomes. The kinetics of association of lipid-free apoA-I with DMPC multilamellar vesicles were followed by the decrease in the turbidity at 325 nm, which reflects the formation of DMPC−apoA-I complexes. These data for WT and each mutant apoA-I are shown in Figure 4, and the half-times ($t_{1/2}$) are listed in Table 3. WT and the Δ(136−143) mutant exhibit similar initial kinetics of association with DMPC liposomes. The Δ(144−165) and L141R mutants show lower initial rates of association with DMPC liposomes than WT, with the lowest rate observed for the Δ(144−165) deletion mutant. In contrast, the E125K/E128K/K133E/E139K mutant shows an increased initial rate of association of apoA-I with DMPC liposomes.

Size of POPC−Cholesterol−ApoA-I Particles Containing WT and Mutant ApoA-I Forms. The apoA-I mutants were used to generate reconstituted POPC−cholesterol−apoA-I particles. Nondenaturing gradient gel electrophoresis verified the formation of the rHDL particles and showed the presence of two bands for the rHDL made with each protein (Figure 5). The ranges of the hydrodynamic diameters of the particles estimated from the gradient gel electrophoresis using high-molecular mass calibration proteins are shown in Table 3. The low intensity of both bands corresponding to rHDL made with the Δ(144−165) mutant indicates a small number of particles formed with this protein, and the smaller size of these particles compared to those made with other recombinant apoA-I suggests the poor ability of this deletion mutant to bind lipids. rHDL made with the E125K/E128K/K133E/E139K mutant are larger than those made with WT and other mutants, although the larger size band for these particles had low intensity. The shape and the average size of the rHDL particles were determined by electron microscopy (Figure 6 and Table 3). Electron micrographs of particles formed by three of the mutants, Δ(136−143), E125K/E128K/K133E/E139K, and L141R, and by WT (Figure 6B−E) show rouleaux, which are indicative of discoidal complexes that stacked on the edge. In contrast, the electron micrographs of the complexes made with the Δ(144−165) mutant (Figure 6A) show a few discoidal particles and large amounts of lipid vesicles. These findings, combined with gradient gel electrophoresis analysis of the particles made with this mutant, indicate that deletion of residues 144−165 impairs the ability of apoA-I to form discoidal particles. The average diameter of the particles made with the Δ(144−165) mutant was not determined from the electron micrographs due to a small number of particles. We did not find a significant effect of the Δ(136−144) or L141R mutation on the size of the discoidal complexes. In contrast, according to the electron microscopy analysis, the average diameter of the rHDL containing the E125K/E128K/K133E/E139K mutant is ∼7 nm larger than that of the rHDL made with WT, in agreement with the increased size of these complexes estimated from gradient gel electrophoresis.

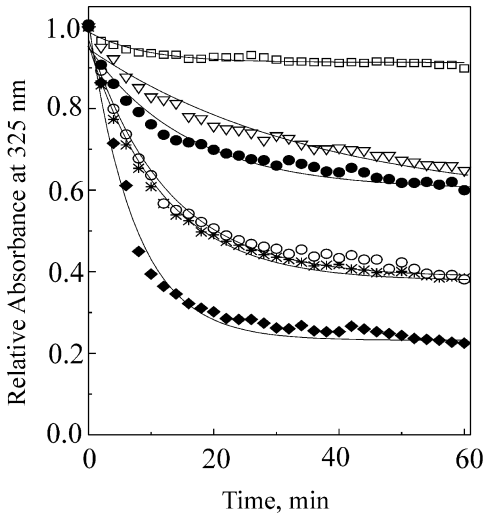

FIGURE 4: Kinetics of DMPC association with recombinant forms of apoA-I as monitored by turbidity changes over time at 24 °C. DMPC multilamellar vesicle dispersion was combined with recombinant apoA-I as described in Materials and Methods: WT apoA-I (∗), Δ(144−165) (▽), Δ(136−143) (○), E125K/E128K/K133E/E139K (◆), and L141R (●). DMPC alone (□). The turbidity was monitored as absorbance at 325 nm at 2 min intervals.

Table 3: Interaction of WT and Variant ApoA-Is with Phospholipids and Half-Times of Association of DMPC with Proteins and POPC−Cholesterol−ApoA-I Particle Size

protein	$t_{1/2}$[a] (min)	diameter[b] (nm)	diameter[c] (nm)	
			smaller size band	larger size band
WT	8.2	12.8 ± 2.2	9.8−10.6	12.0−12.8
Δ(144−165)	25.1***	−	9.3−9.6	10.0−10.7
Δ(136−143)	8.6	13.0 ± 2.6	9.6−10.4	11.4−12.4
E125K/E128K/K133E/E139K	5.0*	19.3 ± 2.9*	11.3−12.5	14−15
L141R	10.9	11.3 ± 1.3	9−10	11−12

[a] Half-times ($t_{1/2}$) of association of DMPC with proteins determined from plots of fractional absorption at 325 nm vs time (minutes) (Figure 4); SD < ±1min for each protein. Significant difference from the value for WT: one asterisk, $p < 0.05$; three asterisks, $p < 0.005$. [b] Average major diameter of rHDL particles determined from electron micrographs of negatively stained samples; the means and standard deviations of the diameters for 100 particles are given. [c] Ranges of the hydrodynamic diameters of rHDL particles estimated from 8 to 25% nondenaturing gradient gel electrophoresis using high-molecular mass calibration proteins.

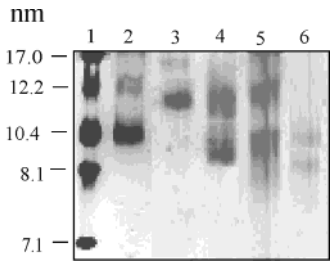

FIGURE 5: Nondenaturing gradient (8 to 25%) gel of rHDL. In lane 1 are high-molecular mass calibration proteins [corresponding Stokes diameters (nanometers) indicated]. POPC−cholesterol−apoA-I complexes were made with WT or one of the mutant apoA-Is: lane 2, WT; lane 3, E125K/E128K/K133E/E139K; lane 4, L141R; lane 5, Δ(136−143); and lane 6, Δ(144−165). Gels were stained for protein.

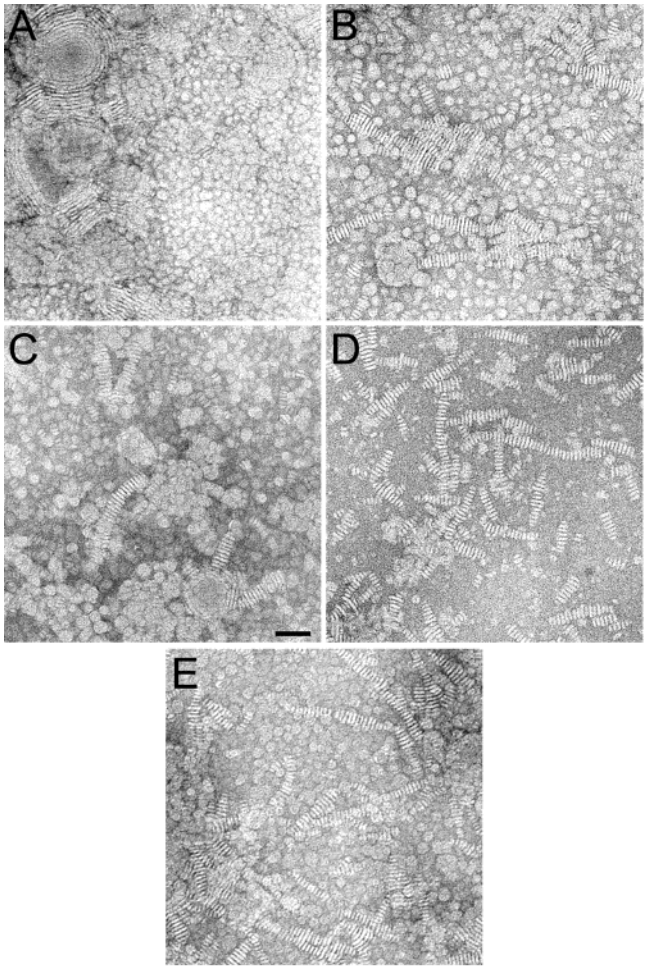

FIGURE 6: Electron microscopy of the negatively stained POPC−cholesterol−apoA-I complexes. The complexes were prepared as outlined in Materials and Methods in the presence of recombinant apoA-I: (A) Δ(144−165), (B) Δ(136−143), (C) E125K/E128K/K133E/E139K, (D) L141R, and (E) WT. All micrographs are shown at a magnification of 90000×. The scale bar corresponds to 25 nm.

DISCUSSION

In our previous study (*15*), we probed the conformation of the C-terminal part (residues 165−243) of lipid-free apoA-I by mutation. The findings were consistent with the secondary structure predicted for this region by Nolte and Atkinson (*16*) (Figure 7, inset). This prediction that was based on the apoA-I sequence and, therefore, reflects the propensity of the sequence to fold into a particular secondary structure was, however, constrained by using the α-helical content data for lipid-bound apoA-I. Therefore, this model should contain more helical segment(s) compared to the secondary structure prediction that would use the α-helical content for the lipid-free protein. Indeed, the model predicts ∼22 additional helical residues compared to the number of helical residues determined for lipid-free plasma apoA-I (168 vs ∼146 residues, respectively) (*15*). This ∼22-residue difference, which corresponds to the number of residues in any of the predicted 22-residue repeats that may form helices, is consistent with a secondary structure of lipid-free apoA-I that differs from the predicted secondary structure of lipid-bound protein by unfolding of one helical segment. We hypothesized that one of the central 20-residue helices predicted by the model (Figure 7, inset) might be unfolded in the lipid-free state. To test this hypothesis, and to probe the secondary structure of the central region of residues 123−165 of lipid-free apoA-I, we mutated this region and studied the effects of the mutation on the conformation and stability of apoA-I, and on the initial rate and capability of the proteins to bind lipids. The results are consistent with a disordered structure of residues 123−142 in lipid-free apoA-I.

The Δ(144−165) mutation deletes residues 145−164 that are predicted to form helix 6 in lipid-bound apoA-I with the adjacent Leu144 and Pro165 (Figure 7, inset). In the lipid-free state, this 22-residue deletion results in a loss of ∼22 residues in the helical conformation (Table 1), suggesting helical structure of the deleted segment. The alternative suggestion of disordered structure of residues 144−165 would imply, in the context of our CD analysis, an indirect effect of the mutation, namely, unfolding of an ∼22-residue helical segment in another part of the mutated protein. That is unlikely, given the molten globular-like state of lipid-free

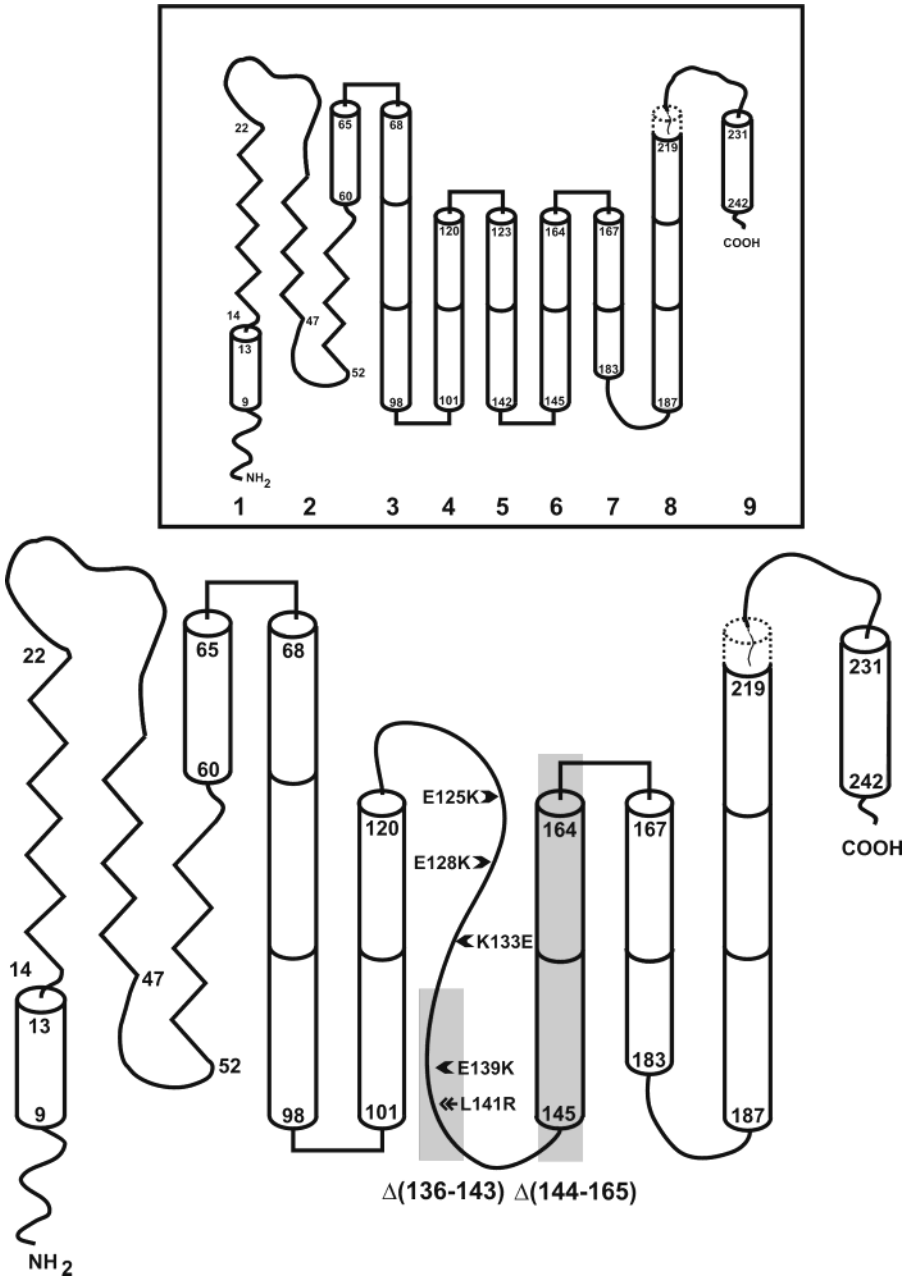

FIGURE 7: Proposed secondary structure model of lipid-free apoA-I. The model has been proposed on the basis of the secondary structure prediction of lipid-bound apoA-I made by Nolte and Atkinson (inset, adopted from ref *16*) and studies of the mutations in the C-terminal (*15*) and central (this study) regions of apoA-I. The model does not address the tertiary conformation. Sites of mutations studied in the current work are shown: (shaded cylinders) internal deletions, (arrowheads) the quadruple-point mutation E125K/E128K/E139K/K133E, and (hatched arrowheads) the L141R point mutation. Underlined numbers on the bottom of the inset indicate the numbers of the corresponding helix in the model of Nolte and Atkinson.

apoA-I in which the helices are only weakly stabilized by tertiary interactions (*37*, *38*). The Δ(144−165) mutation leads to a significant reduction in the protein thermal and chemical stability and unfolding cooperativity, in agreement with the helical structure of the deleted segment. Moreover, the Δ(144−165) deletion is the only mutation studied in this work that leads to a red shift in WMF, indicating a more polar environment of Trp residues in this mutant than in WT and other mutants. Since all the Trp residues are located in the N-terminal half of apoA-I (positions 8, 50, 72, and 108), which is not in the vicinity of the deleted segment in the primary sequence of apoA-I, these observations suggest that the Δ(144−165) deletion affects the tertiary structure of the whole protein or at least its N-terminal half. An organization of the N-terminal half of lipid-free apoA-I in a bundle of helices, as suggested by Davidson et al. (*39*), may be affected by this deletion that, in turn, may lead to the observed more polar environment of Trp residues in the mutant.

The disrupting effect of the Δ(144−165) deletion on the tertiary organization of the N-terminal half of apoA-I is also consistent with the conformational stability of this mutant monitored by fluorescence versus that monitored by CD. Monitoring denaturation by CD at 222 nm reflects changes in the protein overall secondary structure, while monitoring denaturation by Trp fluorescence reflects changes in the secondary and tertiary structure of the N-terminal half of apoA-I, where Trp residues are located. The molten globular state of lipid-free apoA-I suggests noncoincident unfolding

of different secondary and tertiary structural elements of the protein (*37*). For WT and the Δ(136−143), E125K/E128K/K133E/E139K, and L141R mutant forms of apoA-I, monitoring denaturation by Trp fluorescence gives higher values for $\Delta G_D°$ and *m* compared to the corresponding values determined from monitoring by CD for the same protein (Tables 1 and 2). This suggests higher stability of the N-terminal half of the proteins compared to the average stability of the whole protein and may reflect the presence of specific stabilizing secondary and tertiary interactions in the N-terminal half of apoA-I. This is in a good agreement with the organization of the N-terminal half of lipid-free apoA-I suggested by Davidson (*39*). Interestingly, chemical unfolding curves for other apolipoproteins, apoE isoforms, were also different when unfolding was monitored by CD at 222 nm and by Trp fluorescence (*40*). The only protein studied in the present work that exhibits values of $\Delta G_D°$ and *m* that do not depend on whether unfolding is monitored by following Trp fluorescence or CD at 222 nm is the Δ(144−165) mutant. This is consistent with our interpretation that the Δ(144−165) deletion perturbs the organization of the N-terminal half of the protein. This interpretation is also supported by the observation that the effect of the Δ(144−165) mutation on the protein conformational stability $\Delta G_D°$ monitored by Trp fluorescence is significantly larger (2.2 kcal/mol for the mutant vs 4.0 kcal/mol for WT, which is an ∼45% decrease) than that monitored by ellipticity at 222 nm (2.0 kcal/mol for the mutant vs 2.5 kcal/mol for WT, which is an only ∼20% decrease).

The deletion Δ(144−165) that significantly affects the conformation and stability of apoA-I also leads to the most significant reduction in the initial rate of the protein association with DMPC liposomes. This indicates the importance of helix 6 (residues 145−164) for the initial rate of association with phospholipids. The findings are in agreement with data by Frank et al. (*22*), which indicate that helices spanning residues 122−186 contribute to the initial rates of lipid−protein association. Our data suggest that the disturbed organization of the N-terminal half of the protein as a result of the Δ(144−165) mutation may also contribute to the observed reduction in the initial rate of association of apoA-I with DMPC. The abundance of lipid vesicles observed in micrographs of rHDL made with the Δ(144−165) mutant and the relatively small size of the particles estimated from nondenaturing gradient electrophoresis gels indicate the poor ability of the protein to bind to phospholipids. It is believed that the length of the helices (or the number of α-helical segments) in the apoA-I molecule determines the association of the apolipoprotein with lipids (*41*, *42*). Thus, the observed reduced capability of the Δ(144−165) mutant to bind phospholipids is consistent with helical structure of the deleted segment. The observed significant effects of the Δ(144−165) deletion on the conformation, stability, and phospholipid binding properties of apoA-I are consistent with in vitro and in vivo observations suggesting that the repeat 143−164 is responsible for providing an essential protein conformation for the activation of LCAT (*6*, *7*, *18*, *21*, *23*). Sorci-Thomas et al. (*6*) have shown that not only the presence but also the proper alignment and orientation of the hydrophobic face of the repeat 143−164 are important for the LCAT activating ability of apoA-I. However, the authors found that deletion of residues 143−164 led to an ∼0.3 M increase in the midpoint of GdnHCl-induced denaturation of lipid-free apoA-I monitored by CD (*6*), suggesting stabilization of the protein. Given that primary sequences of Δ(144−165) and Δ(143−164) apoA-I are identical, this finding does not agree with the analysis of CD- and fluorescence-monitored chemical unfolding and CD-monitored thermal unfolding performed in this work that all indicate a large destabilizing effect of the Δ(144−165) deletion, consistent with helical structure of the deleted segment.

The eight-residue deletion Δ(136−143) does not affect the number of residues in the helical conformation, suggesting a disordered structure of the deleted segment, which is in agreement with the stabilizing effect of this deletion revealed by monitoring the thermal and chemical unfolding by CD at 222 nm. Interestingly, WMF and the thermodynamic parameters determined from monitoring unfolding by Trp fluorescence are not altered by the Δ(136−143) mutation, indicating that the environment of tryptophans located in the N-terminal part of apoA-I and the stabilizing interactions in the N-terminal part are not affected significantly by this deletion. The Δ(136−143) deletion does not alter the initial rate of association of the protein with DMPC liposomes and the size of POPC−cholesterol−apoA-I particles. This is consistent with the disordered structure of residues 136−143, since the number and length of the helices in apoA-I are not altered by deletion of the disordered segment, and therefore, the association of the protein with lipids is not affected.

The quadruple-point substitution E125K/E128K/K133E/E139K partially reverses the electrostatic charge of residues 123−142, which are predicted to form helix 5 in the lipid-bound state of apoA-I. This mutation was designed to make the charge distribution of the 22-mer repeat 121−142 of apoA-I similar to that of the 22-mer repeat 139−160 of apoE3. The segment of residues 139−160 of apoE3 comprises a central part of the longest helix of the four-helix bundle structure determined by the X-ray crystallographic analysis of the 22 kDa amino-terminal domain of apoE3 that is unusually stable compared to other apolipoproteins (*43*). This segment includes the receptor-binding region of apoE (residues 136−158) that is enriched in basic amino acid residues. It appears that the E125K/E128K/K133E/E139K mutation, which makes the 22-mer repeat 121−142 of the mutant apoA-I also enriched with basic residues, leads to protein stabilization and to an ∼17-residue increase in the number of the protein residues in the helical conformation. These data are consistent with a disordered structure of residues 123−142 of lipid-free apoA-I, which become helical when the quadruple-point mutation is introduced. The additional helical segment in the E125K/E128K/K133E/E139K mutant, compared to WT, leads to the observed increase in the initial rate of association of apoA-I with DMPC liposomes. The increased size of rHDL made with the E125K/E128K/K133E/E139K mutant is also consistent with an additional helical segment in this mutant compared to WT, in accordance with the observation that the number and total length of helices in apolipoproteins determine association of the apolipoproteins with lipids (*41*, *42*). Similar to the stabilization of the structure of the apoE3 22 kDa fragment, interhelical salt bridges and, perhaps, packing of the hydrophobic residues in the interior of the molecule may

contribute to stabilization of the helical structure of the mutated segment of residues 123−142 in the E125K/E128K/K133E/E139K apoA-I.

Thus, the studies presented here, together with our previous findings on the conformation of the C-terminal part of apoA-I (*15*), are consistent with the secondary structure of lipid-free apoA-I that differs from the predicted conformation of the lipid-bound protein (Figure 7, inset) in the unfolding of residues 123−142, as proposed in the model in Figure 7. The proposed model is, however, two-dimensional and does not address the tertiary conformation. Our ongoing studies designed to probe the structure of the N-terminal region of lipid-free apoA-I, together with the existing data that suggest an organization of the N-terminal part of apoA-I in a bundle of helices (*39*) and the proximity of the N- and C-termini of apoA-I in solution (*44*), will be used to propose a more precise three-dimensional model of lipid-free apoA-I. The conformation of the lipid-free E125K/E128K/K133E/E139K mutant, with the helical conformation of residues 123−142, may mimic one of the lipid-bound conformations of apoA-I. A physiological role of the disordered segment of residues 123−142 in the central region of lipid-free apoA-I may be related to the protein conformational plasticity that is essential for protein function and translocation. The structural adaptability of apoA-I and other exchangeable apolipoproteins to heterogeneous lipoproteins and plasma may be attributed to folding−unfolding processes of the protein α-helices. Once lipids are bound, exchangeable apolipoproteins increase their α-helical content by up to 30%, depending on the amount and composition of bound lipids (*6*, *10*, *11*, *13*, *18*, *21*). In apoA-I, residues 123−142 may be one of the segments that change their conformation in the course of HDL metabolism. The relatively low conformational stability of lipid-free apoA-I, along with the absence of strong tertiary interactions and other characteristics of the protein as a molten globule (*13*, *15*, *37*, *38*), facilitates these conformational transitions. If the E125K/E128K/K133E/E139K apoA-I mutant had been selected by evolution due to its higher stability, it would have lower conformational flexibility and structural adaptability than WT.

The disordered structure of residues 123−142 is in excellent agreement with the observed data on the stabilizing effect of the Δ(136−143) mutation. According to our hypothesis, the Δ(136−143) deletion appears to shorten a disordered region of residues 123−142 located in the central part of lipid-free apoA-I. This may bring some groups of the N- and C-terminal halves of apoA-I closer to each other and, thus, facilitate additional stabilizing interactions between them that, in turn, would contribute to the observed stabilization of the Δ(136−143) mutation. The disordered structure of the segment of residues 123−142 agrees with the proteolytic cleavage sites found in the proximity of E125 and E136 of lipid-free apoA-I (*24*) and with immunoreactivity of various parts of the segment of residues 123−142 with antibodies (*45*). It has been shown (*45*) that residues 135−140 form one of few continuous epitopes of apoA-I, and the segments of residues 119−126 and 136−143 that overlap with the segment of residues 123−142 are part of a tertiary discontinuous epitope (along with residues 45−51 and 83−92). Interestingly, among 15 epitopes distributed along the apoA-I sequence, the epitope 4F7 comprising residues 121−141 is the one that exhibits maximal differences in immunoreactivity between the lipid-bound and lipid-free states of the protein (*45*). This agrees with helical structure of residues 123−142 in the lipid-bound state and unfolding of this helix in the lipid-free state of apoA-I.

The substitution of charged Arg for the unpolar and relatively smaller Leu, in L141R, represents a naturally occurring mutation that is associated with coronary heart disease; this mutation has been reported to hamper the ability of apoA-I to promote cholesterol efflux and activate LCAT (*46*, *47*). Our studies show that this single-amino acid substitution does not significantly alter the number of α-helical residues in the lipid-free protein, in agreement with the location of this residue in a disordered segment, and does not affect WMF. However, this mutation destabilizes the protein, suggesting that Leu141 may be involved in a small number of tertiary interactions, such as leucine zipper-like structures (*48*), that may be affected by the mutation. The destabilizing effect of the L141R mutation may also result from new electrostatic interactions created by Arg141 in the mutant protein, which may affect the tertiary conformation and stability of apoA-I without altering the environment of tryptophan residues. This agrees with immunochemical data indicating that the segment of residues 136−143, including Leu141, is a part of a tertiary discontinuous epitope (along with residues 119−126, 83−92, and 45−51) (*45*). Interestingly, deletion of the whole segment of residues 136−143 of this discontinuous epitope increases the protein stability, while a single-point substitution of a charged for an unpolar amino acid in this region (L141R) destabilizes the protein. The L141R mutation leads to a reduction in the initial rate of the association of apoA-I with DMPC liposomes. Again, deletion of the segment of residues 136−143, including L141, does not affect the initial rate of the association of apoA-I with DMPC liposomes. This supports the interpretation that the basic Arg141 residue may affect the tertiary conformation of the protein that is essential for the initial stages of the phospholipid−protein interaction. Although we did not find a significant effect of the L141R mutation on the size of rHDL particles, both electron microscopy and gradient gel electrophoresis analysis of the rHDL show a tendency of this mutation to diminish the size of the particle. The observed reduced stability and the initial rate of association of L141R apoA-I with DMPC liposomes may be related to the altered functions of the mutant protein in vivo.

In conclusion, this work provides new information about the conformation and stability of lipid-free apoA-I that plays a vital role in lipoprotein metabolism. Our data are consistent with the helical structure of the segment of residues 144−165, which is critical for the overall protein conformation, stability, and phospholipid binding ability, and the disordered structure of the segment of residues 123−142 of lipid-free apoA-I, which is likely to become helical upon binding to lipids. Together with the data obtained earlier, the findings of this study suggest that in lipid-free apoA-I, the segment of residues 123−142 may serve as a hinge domain between the N-terminal part proposed by Davidson et al. (*39*) to be organized into a bundle of helices and the C-terminal part that has a stable helical structure. The disordered domain contains a site of the naturally occurring point mutation, L141R, that may affect important functions of apoA-I via reduced stability and phospholipid binding ability of the mutant protein.

ACKNOWLEDGMENT

We are grateful to Donald Gantz for the expert electron microscopy analysis.

REFERENCES

1. Fielding, C. J., and Fielding, P. E. (1995) *J. Lipid Res. 36*, 211−228.
2. Frank, P. G., and Marcel, Y. L. (2000) *J. Lipid Res. 41*, 853−872.
3. Segrest, J. P., Anantharamaiah, G. M., Harvey, S. C., Liadali, K. N., and Zannis, V. (2000) *Curr. Opin. Lipidol. 11*, 105−115.
4. Rothblat, G. H., de la Llera-Moya, M., Atger, V., Kellner-Weibel, G., Williams, D. L., and Phillips, M. C. (1999) *J. Lipid Res. 40*, 781−796.
5. Leroy, A., Toohill, K. L. H., Fruchart, J.-C., and Jonas, A. (1993) *J. Biol. Chem. 268*, 4798−4805.
6. Sorci-Thomas, M. G., Currtiss, L., Parks, J. S., Thomas, M. J., Kearns, M. W., and Landrum, M. (1998) *J. Biol. Chem. 273*, 11776−11782.
7. Sorci-Thomas, M. G., Thomas, M., Curtiss, L., and Landrum, M. (2000) *J. Biol. Chem. 275*, 12156−12163.
8. Sviridov, D., Hoang, A., Sawyer, W. H., and Fidge, N. H. (2000) *J. Biol. Chem. 275*, 19707−19712.
9. De Beer, M. C., Durbin, D. M., Cai, L., Jonas, A., de Beer, F. C., and van der Westhuyzen, D. R. (2001) *J. Lipid Res. 42*, 309−313.
10. Sparks, D. L., Lund-Katz, S., and Phillips, M. (1992) *J. Biol. Chem. 267*, 25839−25847.
11. Sparks, D. L., Lund-Katz, S., Davidson, W. S., and Phillips, M. (1995) *J. Biol. Chem. 270*, 26910−26917.
12. Tricerri, M. A., Agree, A. K. B., Sanchez, S. A., Bronski, J., and Jonas, A. (2001) *Biochemistry 40*, 5065−5074.
13. Brouillette, C. G., Anantharamaiah, G. M., Engler, J. A., and Borhani, D. W. (2001) *Biochim. Biophys. Acta 1531*, 4−46.
14. Rogers, D., Roberts, L. M., Lebowitz, J., Datta, G., Anantharamaiah, G. M., Engler, J., and Brouillette, C. G. (1998) *Biochemistry 37*, 11714−11725.
15. Gorshkova, I. N., Liadaki, K., Gursky, O., Atkinson, D., and Zannis, V. I. (2000) *Biochemistry 39*, 15910−15919.
16. Nolte, R. T., and Atkinson, D. (1992) *Biophys. J. 63*, 1221−1239.
17. Borhani, D. W., Rogers, D. P., Engler, J. A., and Brouilette, C. G. (1997) *Proc. Natl. Acad. Sci. U.S.A. 94*, 12191−12296.
18. Sorci-Thomas, M. G., Curtiss, L., Parks, J. S., Thomas, M. J., and Kearns, M. W. (1997) *J. Biol. Chem. 272*, 7278−7284.
19. Lindholm, E. M., Bielicki, J. K., Curtiss, L. K., Rubin, E. M., and Forte, T. M. (1998) *Biochemistry 37*, 4863−4868.
20. Dhoest, A., Zhao, Z., De Giest, B., Deridder, E., Sillen, A., Engelborghs, Y., Collen, D., and Holvoet, P. (1997) *J. Biol. Chem. 272*, 16967−16972.
21. Roosbeek, S., Vanloo, B., Duverger, N., Caster, H., Breyne, J., De Beum, I., Patel, H., Vandekerckhove, J., Shoulders, C., and Rosseneu, M. (2001) *J. Lipid Res. 42*, 31−40.
22. Frank, P. G., Bergeron, J., Emmanuel, F., Lavigne, J.-P., Sparks, D. L., Denefle, P., Rassart, E., and Marcel, Y. (1997) *Biochemistry 36*, 1798−1806.
23. McManus, D. C., Scott, B. R., Frank, P. G., Franklin, V., Schultz, J. R., and Marcel, Y. L. (2000) *J. Biol. Chem. 275*, 5043−5051.
24. Roberts, L. M., Ray, M. J., Shih, T.-W., Hayden, E. H., Reader, M. M., and Brouillette, C. G. (1997) *Biochemistry 36*, 7615−7624.
25. Liadaki, K. N., Liu, T., Xu, S., Ishida, B. Y., Duchateaux, P. N., Krieger, J. P., Kane, J., Krieger, M., and Zannis, V. I. (2000) *J. Biol. Chem. 275*, 21262−21271.
26. Sorci-Thomas, M. G., Parks, J. S., Kearns, M. W., Pate, G. N., Zhang, C., and Thomas, M. (1996) *J. Lipid Res. 37*, 673−683.
27. Crowe, J., Masone, B. S., and Ribbe, J. (1996) *Methods Mol. Biol. 58*, 491−510.
28. Dougherty, W. G., Carrington, J. C., Cary, S. M., and Parks, T. D. (1988) *EMBO J. 7*, 1281−1287.
29. Carrington, J. C., and Dougherty, W. G. (1988) *Proc. Natl. Acad. Sci. U.S.A. 85*, 3391−3395.
30. Donovan, J. M., Benedek, G. B., and Carey, M. C. (1987) *Biochemistry 26*, 8116−8125.
31. Chen, Y.-H., Yang, J. T., and Martinez, H. M. (1972) *Biochemistry 11*, 1420−1431.
32. Pace, C. N., Shirley, B. A., and Thomson, J. A. (1989) in *Protein Structure* (Creigton, T. E., Ed.) pp 311−330, IRL Press, New York.
33. Pace, C. N., and Vanderburg, K. E. (1979) *Biochemistry 18*, 288−292.
34. Pownall, H. J., Massey, J. B., Kusserov, S. K., and Gotto, A. M. (1978) *Biochemistry 17*, 1183−1188.
35. Matz, C. E., and Jonas, A. (1982) *J. Biol. Chem. 257*, 4535−4540.
36. Xu, S., Laccotripe, M., Huang, X., Rigotti, A., Zannis, V. I., and Krieger, M. (1997) *J. Lipid Res. 38*, 1289−1298.
37. Gursky, O., and Atkinson, D. (1996) *Proc. Natl. Acad. Sci. U.S.A. 93*, 2991−2995.
38. Rogers, D. P., Roberts, L. M., Lebowitz, J., Engler, J. A., and Brouilette, C. G. (1998) *Biochemistry 37*, 945−955.
39. Davidson, W. S., Arnvig-McGuire, K., Kennedy, A., Kosman, J., Hazlett, T. L., and Jonas, A. (1999) *Biochemistry 38*, 14387−14395.
40. Morrow, J. A., Segall, M. L., Lund-Katz, S., Phillips, M. C., Knapp, M., Rupp, B., and Weigraber, K. H. (2000) *Biochemistry 39*, 11657−11666.
41. Jonas, A., Kezdy, K. E., and Wald, J. H. (1989) *J. Biol. Chem. 264*, 4818−4824.
42. Segrest, J. P., Garber, D. W., Brouillettee, C. G., Harvey, S. C., and Anantharamaian, G. M. (1994) *Adv. Protein Chem. 45*, 303−369.
43. Weisgraber, K. H. (1994) *Adv. Protein Chem. 45*, 249−302.
44. Tricerri, M. A., Behling Agree, A., Sanchez, S. A., and Jonas, A. (2000) *Biochemistry 39*, 14682−14691.
45. Calabresi, L., Meng, Q.-H., Castro, G. R., and Marcel, Y. L. (1993) *Biochemistry 32*, 6477−6484.
46. Miccoli, R. A., Bertolotto, J. K., Goth-Goldstein, R., Selmek, J., and McCall, M. R. (1996) *Circulation 94*, 1622−1628.
47. Miccoli, R. A., Zhu, H., Daum, U., Wessling, J., Huang, Y. D., Navalesi, R., Assmann, G., and Von Eckardstein, A. (1997) *J. Lipid Res. 38*, 1242−1253.
48. Landschulz, W. H., Johnson, P. F., and McKnight, S. L. (1988) *Science 240*, 1759−1764.

BI025807D